SANDIA REPORT

SAND2009-6799

Unlimited Release

October 2009

Calibration of an Interfacial Force Microscope for MEMS Metrology: Activities in FY08-09

Nathan W. Moore, Douglas A. Crowson, Jack E. Houston,

John A. Mitchell, Michael S. Baker

Prepared by
Sandia National Laboratories
Albuquerque, New Mexico 87185 and Livermore, California 94550

Sandia is a multiprogram laboratory operated by Sandia Corporation,
a Lockheed Martin Company, for the United States Department of Energy's
National Nuclear Security Administration under Contract DE-AC04-94AL85000.

Issued by Sandia National Laboratories, operated for the United States Department of Energy by Sandia Corporation.

Available to DOE and DOE contractors from

U.S. Department of Energy
Office of Scientific and Technical Information
P.O. Box 62
Oak Ridge, TN 37831

Telephone: (865) 576-8401
Facsimile: (865) 576-5728
E-Mail: reports@adonis.osti.gov
Online ordering: http://www.osti.gov/bridge

Available to the public from

U.S. Department of Commerce
National Technical Information Service
5285 Port Royal Rd.
Springfield, VA 22161

Telephone: (800) 553-6847
Facsimile: (703) 605-6900
E-Mail: orders@ntis.fedworld.gov
Online order: http://www.ntis.gov/help/ordermethods.asp?loc=7-4-0#online

SAND2009-6799
Unlimited Release
October 2009

Calibration of an Interfacial Force Microscope for MEMS Metrology: FY08-09 Activities

Nathan W. Moore, Douglas A. Crowson, Jack E. Houston

Surface and Interface Science Department

John A. Mitchell

Electromechanical Engineering Department

Michael S. Baker

MEMS Technologies Department

Sandia National Laboratories
P.O. Box 5800
Albuquerque, New Mexico 87185-MS1415

Abstract

Progress towards a NIST-traceable calibration method is described for a next-generation, 2D Interfacial Force Microscope (IFM) for applications in MEMS metrology and qualification. Discussed are the results of screening several suitable calibration methods and the known sources of uncertainty in each method.

CONTENTS

FIGURES

TABLES

1. INTRODUCTION

1.1 Motivation

Progress in MEMS fabrication has enabled a wide variety of force and displacement sensing devices to be constructed. One device under intense development at Sandia is a passive shock switch, described elsewhere (Mitchell 2008). A goal of all MEMS devices, including the shock switch, is to achieve a high degree of reliability. This, in turn, requires systematic methods for validating device performance during each iteration of design. Once a design is finalized, suitable tools are needed to provide quality assurance for manufactured devices. To ensure device performance, measurements on these devices must be traceable to NIST standards. In addition, accurate metrology of MEMS components is needed to validate mechanical models that are used to design devices to accelerate development and meet emerging needs.

Few tools exist to accurately and reliably measure the mechanical performance of in-plane MEMS devices (e.g., Chang 2004, Qiu 2001, Qiu 2004). For the shock switch, the requirements are more challenging, owing to its operation in the near- micro-Newton force regime. In addition, the shock-switch is a bistable spring device, which precludes characterization by traditional micromechanics tools. Toward that end, initial measurements demonstrated that the Sandia-developed Interfacial Force Microscope (IFM) could be used to provide detailed information regarding the shock switch's mechanical performance (Mitchell 2008). Thus began an intense effort to employ a next-generation, 2D IFM suitable for performing rapid, fully-calibrated metrology of MEMS devices. Critical to the success of this MEMS metrology effort is the development of robust methods for calibrating the 2D, IFM force sensor, as the low-force operating regime presents unique challenges that have not been previously addressed. This report describes initial progress toward this goal.

A summary of initial measurements on the shock switch and model comparison is published elsewhere (Brake 2009).

A more detailed evaluation of the IFM sensor performance characteristics will be reported separately (Moore 2009).

1.2 Summary of Goals and Progress

Table 1 summarizes the strategy and progress of the instrument development and calibration activities as presently envisioned.

Table 1: Overview of instrument development and calibration

Task	Status
Develop an IFM sensor with adequate sensitivity and repeatability for in-plane measurements of MEMS components	Completed 2008
Integrate the IFM sensor into a measurement platform with automated tip positioning.	Platform completed 2008; refinements ongoing
Demonstrate measurement capabilities on the shock switch	Completed 2008
Screen suitable calibration methods	Completed 2009
Detailed study of calibration uncertainties (e.g., sensor-to-sensor variability, operating conditions, environment, etc.)	Key limitations were identified based on initial screening of techniques, 2009
Minimize calibration error to achieve evolving qualification needs	In progress
Ensure NIST traceability	Collaboration with NIST has been continuous throughout the project.
Certification by Sandia Primary Standards Laboratory	N/A

1.3 Collaboration with the National Institute of Standards

To work toward developing a NIST traceable calibration, a collaboration was initiated with Jon Pratt (NIST, Manufacturing Engineering Division). Interactions included:

- site visit to NIST (Maryland) by Jack Houston in 2008
- site visit to SNL/NM by Jon Pratt, c.a. March 2009
- one-day focus workshop with attendees from the IFM group, shock switch group, SNL Primary Standards Laboratory, and Jon Pratt (NIST) (Jan. 22, 2009)
- provision of NIST-calibrated cantilevers to the IFM group.

In principle, the cantilevers provided by NIST could be used as force “standards” to calibrate the IFM sensor with higher accuracy than cantilevers that are commercially available (see Section 2.3), by pushing the IFM probe against a cantilever of known stiffness. These cantilevers were calibrated at NIST using a unique instrument in Pratt’s laboratory constructed for this purpose.

Although these cantilevers are not presently identified as “NIST-traceable”, they provide a strong link to the efforts at NIST to develop NIST-traceable standards for micromechanical instruments, such as the IFM. In addition to aiding our own efforts, such interactions provide valuable feedback to NIST during the development of such standards.

1.4 Instrument Description

The IFM instrument revision used in this study will be detailed separately and is summarized in (Mitchell 2008, pp. 71–80). A brief description follows to explain the calibration methods and goals. A second-generation Interfacial Force Microscope adapted from the original design (Joyce and Houston 1991, Houston and Michalske 1992) was developed to allow simultaneous and independent measurement of forces normal and lateral to a sensing probe tip. The instrument is distinguished from other in-plane force sensing methods by its force-feedback mechanism that prevents the mechanical instability inherent in cantilever-based force sensors. As a result, the compliance of a bistable MEMS device, such as the shock switch (Mitchell 2008), can be measured over its entire range of motion, with no gaps in the force-displacement curve. The instrument is also unique in achieving lower force sensitivity than other instruments designed for MEMS metrology.

The force sensor used here is described in (Houston and Smith 2004). In short, the sensor consists of a “teeter totter”-like, silicon top plate suspended on torsion bars above two gold capacitor pads deposited in wells etched into a Pyrex substrate (Fig. 1a,b). The top-plate and substrate are anodically bonded, forming a capacitor gap of ~6 μm. The finished sensor is ~1 cm^2. A sharp tip is placed in the middle of the teeter totter so that a lateral force applied to the tip rotates the top-plate along the torsion bar axis, while a normal force displaces the top-plate vertically. In both cases, the top-plate motion is detected by two laser interferometers (780 nm) aligned near the center of each capacitor pad (Fig.1a). Applying voltage to each pad with the aid of two independent PID controllers keeps the teeter totter balanced in its original position. Because electrostatic forces are always attractive, both capacitor pads require a bias voltage (V_0) to measure repulsive forces.

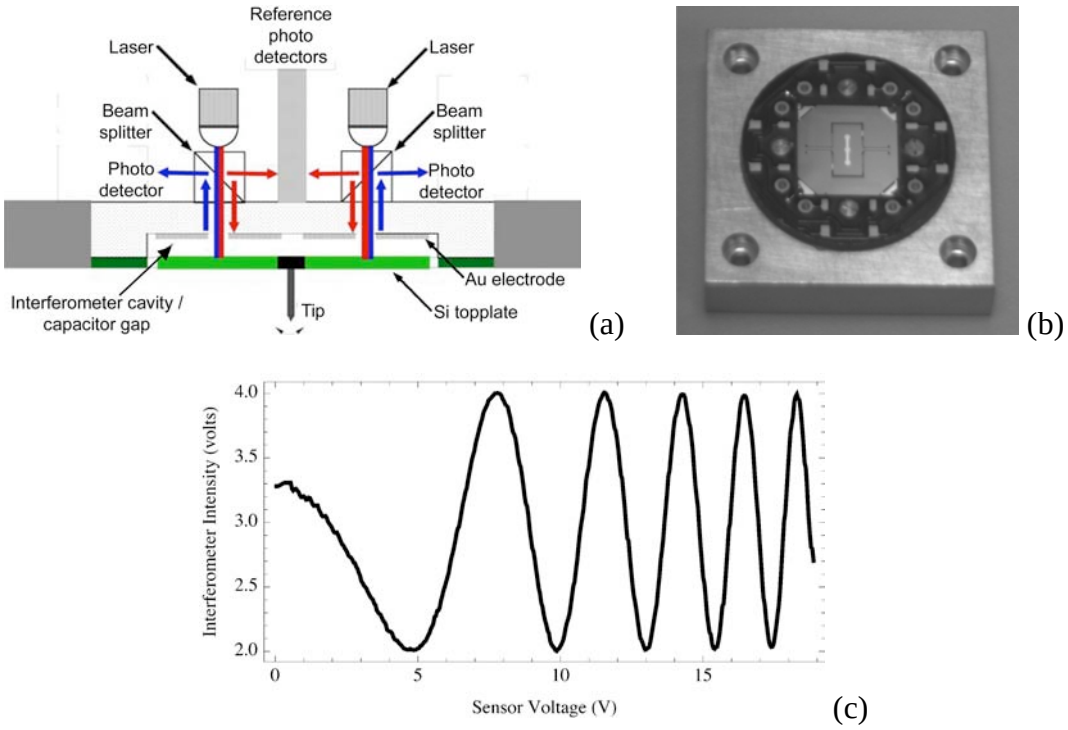

Figure 1. (a) Schematic (side-view) of the laser interferometer sensor. (b) Top view of the sensor assembled onto a fiberboard housing and temporary aluminum holder (image ~3x3 cm^2). The teeter-totter is etched into the Si topplate shown at the image center. (c) Example of intensity variation on one of the photodiode detectors as the sensor bias voltage is swept, viz., as the gap spacing is changed.

To establish the PID setpoint, the voltage of the two pads are swept while recording the voltage on the photodiode receiving the interferometer light output. By inspecting the resulting interference pattern (Fig.1c), a photodiode voltage setpoint can be chosen at the inflection point nearest the pad bias ($V_{0,i}$) desired for the measurement. With this scheme, the output voltage of each photodiode is roughly proportional to the top-plate displacement and displacement sensitivity is maximized. Thus, the tip force is automatically balanced by the applied electrostatic force and the sensor is mechanically stable. The response time of the sensor under feedback control (~200 μsec) is fast enough to obtain equilibrium force-displacement curves of a MEMS shock switch with a cycle time of ~1 min. per device. The displacement of the tip is controlled with a NanoCube (Princeton Instruments), which is factory calibrated to provide ~1 nm displacement resolution (~ ±2%). Optical microscopes allow manual alignment of the tip with the MEMS device being tested. An automated alignment strategy is presented in (Jones 2000).

Normal (F_N) and lateral (F_L) forces are quantified by taking the sum or difference (respectively) of the electrostatic force (F_i) that is applied to each pad to keep the sensor balanced under feedback, viz.,

$$F_N = F_1 + F_2 \tag{1}$$

$$F_L = (F_1 - F_2)/l \quad (2)$$

where l is the tip length, as the latter is related to the torque applied to the tip end. This force is related to the pad voltages (V_i) as the derivative of the resulting electrostatic energy (E_i), viz.,

$$F_i = -dE_i/dz = -d(C_i V_i^2/2)/dz = \varepsilon_0 A V_i^2/(2d_i^2) = K_i' V_i^2 \quad (3)$$

where z is the coordinate normal to the pad, C_i is the capacitance of pad i, ε_0 is the free-space permittivity, d_i is the gap spacing, and A is the pad area. The K_i' term is the force constant, which is what is needed to calibrate the sensor. In principle, the value, K_i', may be different for each pad because of fabrication errors or from an imbalance in the top-plate orientation. The calibration constant depends strongly on the bias voltage (V_0) on each pad, so that a useful calibration will determine $K_i = f(V_{0,i})$ over the full range of $V_{0,i}$ employed during a measurement. However, it is more convenient to assume $K_1 = K_2$ and then determine the calibration constant under the same operating conditions as the measurements of interest, so that differences between each K_i are subsumed in the calibration and do not introduce error. This assumption is made in all data presented here.

Appendix A lists the procedure used for the demonstration measurements on the MEMS shock switch, using the instrument control software at time of measurement described in Appendix B. A summary of initial measurements on the shock switch, and model comparison, will be published elsewhere (Brake 2009).

1.5 Variability Common to Each Calibration Method

In addition to the accuracy limitations of each calibration method discussed in Section 2, Table 2 lists sources of measurement variation that affect the repeatability of all calibration methods. Although the instrument has been designed to minimize the influence of some of these sources of variability, not all of these uncertainties, nor their collective effects, have been quantified. Such minor influences may be significant in combination when strict calibration tolerances are required. A more detailed evaluation of the sensor performance will be reported separately (Moore 2009).

Table 2: Sources of variability common to each calibration method

Category	Notes
Sensor gap spacing	The measured interference pattern changes frequently (e.g., due to thermal expansion of sensor / laser optics); variability in calibrating over the range of $V_{0,i}$ has not been quantified.
Measurement speed	The measured force can be up to ~5% smaller at fast measurement speeds (> ~100 nm/s), possibly from lag in either the sensor output or displacement control.
Tilt between tip and sample, and between tip and sensor	Distorts lateral force measurement systematically, and can impose torque on sensor in the direction not measurable with a 2D sensor. Can be alleviated by calibrating against an in-plane force gauge in situ with sample. Also minimized by using a cylindrical tip for in-plane measurements.
Sensor fabrication	Sensor-to-sensor variability has not been evaluated from a calibration standpoint.
Sensor mounting	Removing, then reinstalling, a sensor changes the interference pattern, and possibly the calibration.
Sample mounting	Removing, then reinstalling, a sample (shock-switch) showed <5% change in the measured force values; however, this variation has not been rigorously quantified.
Rotation of sample relative to measurement direction	Systematic error (< a few percent). Alleviated by calibrating against an in-plane force gauge in situ with sample.
Temperature	The sensor head assembly is highly sensitive to small temperature changes (e.g., a 1-sec. burst of 15°C air applied to the sensor assembly 6” above the sensor topplate resulted in a ~2% offset in the sensor force output).

2. CALIBRATION METHODS AND RESULTS

2.1 Summary

Table 3 summarizes the five calibration methods that were tested, and for each, a short description, their primary limitation, and the calibration accuracy given the present methods employed. Details of each method are elaborated in the following subsections. In total, approximately 25 sensors have been tested with ~10 tips, encompassing multiple sensor design revisions over the project period. Further, these methods have only been tested over a limited range of operating conditions, so that the accuracies reported are only an estimate from a limited number of measurements. Consequently, the reported accuracies do not represent the limit of each technique; rather, only of what has been measured to date with the present instrument configuration.

Table 3: Calibration methods tested, accuracy estimates, and limitations

Name	Short Description	Accuracy	Primary limitation
In-plane force gauge	Tip is pressed into a linear, microfabricated force gauge.	±18%	Uncertainty in the force gauge spring constant
Out-of-plane cantilever	Tip is pressed against a cantilever standard.	±(6–50)%*	Tip placement accuracy; cantilever calibration
Internal Mass	Sensor/tip assembly is inverted 180º.	±20%	Drift in the sensor's force output
External Mass	A small mass is placed onto the sensor.	N/A	Difficult to place weight without destabilizing the sensor
Capacitive	Sensor capacitances are continuously monitored.	N/A	Electronics prototyped only; an external standard is still required to initially validate the method.

* depending on the cantilever standards and measurement procedure (see Section 2.3).

2.2 In-Plane Force Gauge

In this calibration method, the tip was pushed against a linear force gauge fabricated onto the same die as the MEMS structures to be tested. This was done in the lateral (in-plane) direction relevant to MEMS testing, with an acid-etched, tungsten tip attached to the IFM sensor. The accuracy of this calibration is limited by estimation of the force gauge spring constant (9.6±1.7 N/m), or ~18%, as determined by incorporating known dimensional uncertainties of the fabrication into a finite element model. This method assumes the force constants are the same on each capacitor pad; however, error in that assumption is systematically cancelled by calibrating in the same orientation as the measurement. Figure 2 shows an example of this calibration scheme. In the force range of the gauge (0–80 μN), the lateral force (F_L) measured with our force sensor was approximately linear with respect to the sensor output voltage (V) (R^2=0.99), owing to the small voltage change ($V–V_0 \approx 8$V) relative to the initial bias ($V_0 \approx 25$V). The resulting lateral force calibration gives $K/l = F_L/V = 8.9\pm1.6$ μN/V.

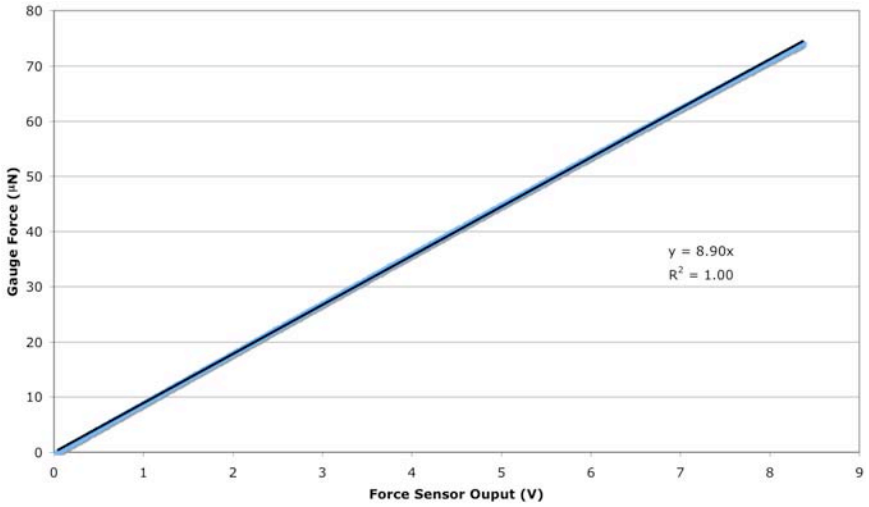

Figure 2. Example calibration using an in-plane, linear force gauge. Shown is the IFM sensor output in the lateral direction (abscissa) against the gauge force (ordinate) calculated from the force gauge spring constant and the known displacement. Data shown in blue; line is a best-fit.

It is recommended to develop a two-sided force gauge so that calibration could be performed by pushing on either side of the force gauge. It may also be necessary to characterize the rate dependence of this calibration technique when high throughput is needed, as preliminary measurements show a ~5% reduction in measured force for measurement speeds > ~100 nm/s. Contact mechanics (friction, stiction, and adhesion) between the sensing probe tip and the cantilever are scale-dependant effects that may also contribute error in this technique in the low-force regime (Matei 2006).

2.3 Out-of-Plane Cantilever

In this calibration method, an IFM tip was pressed against a microfabricated, silicon cantilever of known stiffness, similar to force-sensing cantilevers used in atomic force microscopy, but without a probe tip attached to the reference cantilever. These measurements were done in the direction normal to the substrate, orthogonal to the direction of an actual measurement of a MEMS device. Measurements were made using one of a series of commercially available cantilevers (Applied Nanostructures, Santa Clara, CA; Model FCL; for the series, lengths range 52–422 μm, spring constants range 0.12–77 N/m, and resonant frequencies range 14–1000 kHz). Although these cantilevers are sold as "calibration cantilevers", the manufacturer reports the uncertainty in their factory calibration to be ~ ±50%, which is by far the dominant uncertainty. The accuracy of this calibration method could be improved by pushing the tip against a cantilever that has been calibrated more accurately. Jon Pratt (NIST) has supplied such cantilevers (manufactured by Veeco but calibrated at NIST to ~ ±6%). While these cantilevers have not yet been tested on the IFM system, this represents an obvious route to achieving substantially improved calibration accuracy. Pratt's concept is for the IFM to be calibrated against these cantilevers before the cantilever spring constant is revealed, so that the calibration can be performed in the typical fashion of a "blind" test.

Below is a list of additional challenges of calibrating against a cantilever that have been identified but not quantified:

- Alignment optics limit accuracy in placing the tip a known distance from the cantilever's fulcrum. This can be significant because the calibration accuracy is reduced by the cube of the positioning error. For example, a 5-μm positioning error on a 100-μm calibration cantilever produces a 16% error in calibration due to positioning alone, while a 1-μm positioning error produces still 3% calibration error, in addition to other error sources.
- Alignment optics limit accuracy in placing the tip in the center of the cantilever's width, causing undesirable twist in the cantilever (Matei 2006).
- Contact mechanics (friction, stiction, and adhesion) between the sensing probe tip and the cantilever are scale-dependant effects that should be minimized when the calibration must be executed in the low-force regime (Matei 2006).
- Cantilevers with the appropriate combination of stiffness, length, spacing, and orientation are not always commercially available; however, in principle, they could be fabricated as needed.

2.4 Internal Mass

In this technique, the tip and sensor are inverted 180º, so that the weight of the tip on the sensor acts as a built-in ("internal") force standard, with the measured force equaling twice the weight of the tip. This technique is appealing from a calibration standpoint, as gravimetric techniques are well-established for many larger-scale, force-measuring instruments, such as laboratory scales. In principle, the tip and the epoxy that binds the tip to the sensor could be massed on a NIST-traceable laboratory scale; however, the small combined mass (<20 μg) precludes high

precision. Mass estimates to ~ ±10% can be made based on measuring the tip/epoxy volumes and their known densities.

An additional ~ ±20% uncertainty is introduced by drift in the sensor's force output. This is shown by example in Fig.3a. Here, the sensor/tip assembly was inverted and righted repeatedly, every ~20 min. While the inversion is rapid (~30 sec.), the sensor's force output changes rapidly for the first few minutes, then slowly for another ~10–15 min. Because the origin of this effect is presently unknown, the uncertainty in this method was estimated as the difference in force constant determined before and 20 min. after inverting the sensor. Eliminating the source of this drift could provide a calibration route with accuracy that competes with that of the above in-plane force gauge and cantilever calibration methods.

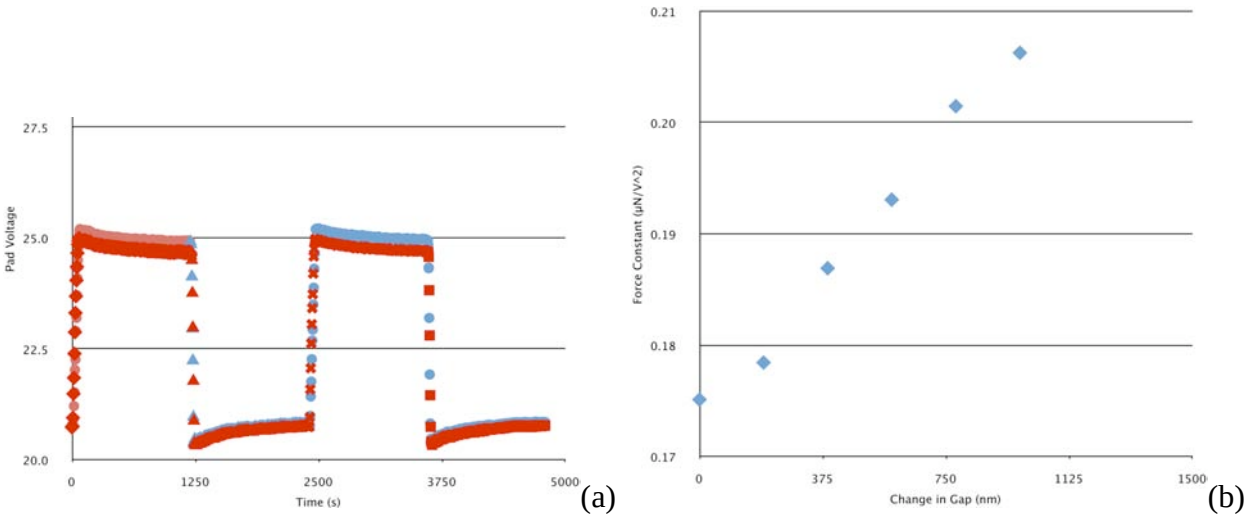

Figure 3. Example calibration data using the tip as an internal mass standard, by repeatedly rotating the sensor/tip assembly 180º. (a) Superimposed (nearly coincident) are the voltages on each pad (V_i) output by each PID to keep the sensor balanced during and after the rotation. The four nearly vertical data streams correspond to when the sensor/tip assembly was inverted. (b) Resulting force constants at different gap spacings, controlled by changing the bias voltage ($V_{0,i}$) on each pad by equal amounts.

Another uncertainty in this technique is illustrated in Fig.3(b). It is seen that the force constant changes nearly linearly with the size of the capacitor gap, which contrasts with the quadratic relationship of Eq.3. Additional study is needed to determine if this non-parabolic relationship arises from variation in the calibration method (e.g., owing to the aforementioned sensor drift) or if the analytical model (Eqs.1–3) for the sensor needs revision to account for manufacturing errors, etc.

A variation of this method is to spin the entire tip/sensor assembly through 360º on a goniometer, and to record the sensor force output as a function of the tilt angle with respect to the earth's center. An example is shown in Fig.4, for both normal (sum) and lateral (difference) force

components. In principle, this provides more information than the one-point calibration described above (180° inversion), but requires an additional fit parameter (the tip's center of gravity) and is subject to the same uncertainties induced by drift in the sensor's force output.

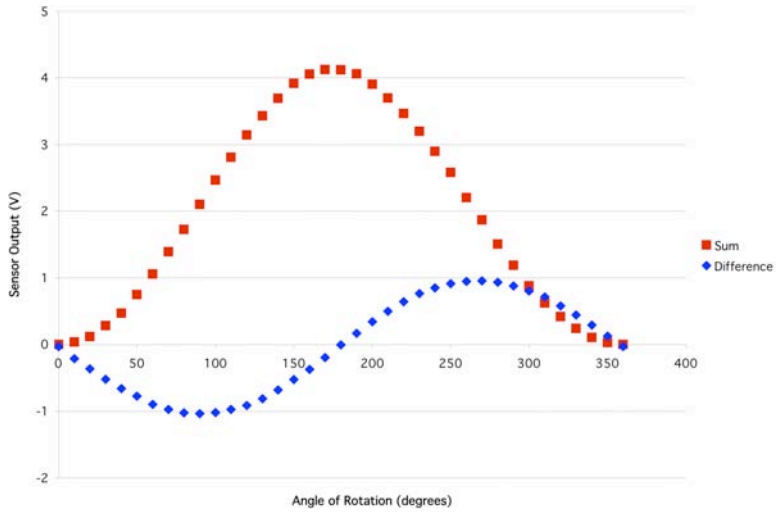

Figure 4. Example calibration data using the tip as an internal mass standard, by rotating the sensor/tip assembly 360º. Shown is the sum (red) and difference (blue) of the voltage on each pad (V_i) output by each PID to keep the sensor balanced during the rotation. Approximately 1 min. elapsed between each data point.

2.5 External Mass

Another gravimetric calibration that was examined was to place a small weight onto the sensor top-plate when the sensor is inverted. The error in this technique has not yet been quantified, owing to implementation difficulties. In short, when the mass is placed too abruptly, the sensor destabilizes, that is, the PID follows a setpoint at the same voltage on an inflection point near an adjacent interference fringe (Fig.1). It may be possible to overcome this difficulty using a micrometer stage to gently place a weight on the topplate in a measurable location.

2.6 Capacitive

An alternative to regularly calibrating with an external reference is to continuously measure the sensor capacitance using a method described in (Mitchell 2008, pp. 76–79). The method is similar to how force measurement is made with analytical laboratory balances with micro-Newton sensitivity. The electronics for this method have been prototyped but not yet validated. This method still requires initial validation using an external calibration method, such as those

described above, to ensure NIST traceability. Nonetheless, this method holds promise as a way to rapidly check the calibration and/or stability of the sensor during its operation.

3. CONCLUSIONS

The choice of calibration method ultimately depends on specific application requirements. Therefore, this report was intended only to summarize possible routes for calibration. In particular, the sources of measurement variability listed in Table 2, as well as those specific to each method, need to be quantified more rigorously before a calibration method can be certified to a given accuracy, and the most appropriate calibration method chosen. Each calibration method is expected to achieve accuracy ~ ±20% without extensive development, which may be adequate for proof-of-concept metrology and failure-analysis settings. However, a rigorous effort may be required to quantify and improve this accuracy to the level needed for MEMS qualification in a post-production setting. Therefore, additional study will be required to develop and certify a calibration method for MEMS qualification. Because no standard calibration method presently exists for this class of instrument, the development of several calibration methods will enhance surety in the calibration result.

4. REFERENCES

M.R. Brake, M.S. Baker, N.W. Moore, D.A. Crowson, J.A. Mitchell, and J.E. Houston, "Modeling and Measurement of a Bistable Beam in a Microelectromechanical System," submitted to Journal of Microelectromechanical Systems, 2009.

K.-K. Chang, N.-C. Shie, H.-M. Tai, and T.-L. Chen, A micro force sensor using force-balancing feedback control system and optic-finger interferometers, Tamkang Journal of Science and Engineering, vol. 7, pp. 91–94, 2004.

S. A. Joyce and J. E. Houston, A new force sensor incorporating force-feedback control for interfacial force microscopy," Rev. Sci. Instrum., vol. 62, pp. 710–715, 1991.

J. E. Houston and T. A. Michalske, The interfacial-force microscope," Nature, vol. 356, pp. 266–267, 1992.

J. E. Houston and W. L. Smith, Laser Interferometry Force-Feedback Sensor for an Interfacial Force Microscope, US Patent 6 718 821, April 13, 2004.

G.D. Jones, J.E. Houston and K.T. Gillen, Method for Accurately Positioning a Device at a Desired Area of Interest, US Patent 6 085 581, July 11, 2000.

G.A. Matei, E.J. Thoreson, J.R. Pratt, D.B. Newell, N.A. Burnham, Precision and accuracy of thermal calibration of atomic force microscopy cantilevers, Rev. Sci. Instrum., 77(8), pp. 083703, 2006.

J.A. Mitchell, M.S. Baker, J. Blecke, R.C. Clemens, D.A. Crowson, D.S. Epp, J.E. Houston, J.A. Walraven, J.W. Wittwer, The Sandia MEMS Passive Shock Sensor: FY07 Maturation Activities, SAND2008-5185. Sandia National Laboratories, Albuquerque, NM, 2008.

N.W. Moore, D.A. Crowson, C.Gutierrez, Initial Evaluation of a 2D Laser-Interferometer Sensor for an Interfacial Force Microscope, SAND Report, in preparation, Sandia National Laboratories, Albuquerque, NM, 2009.

J. Qiu, J. H. Lang, and A. H. Slocum, A curved-beam bistable mechanism, J. Microelectromechanical Systems, vol. 13, pp. 137–146, 2004.

J. Qiu, J. Sihler, J. Li, V. Sturgeon, M. Smith, and A. Slocum, An instrument to measure the stiffness of MEMS mechanisms, Proceedings of the 10th International Conference on Precision Engineering, Yokohama, Japan, July 2001, pp. 599–603.

APPENDIX A: SHOCK SWITCH MEASUREMENT PROCEDURE

The following is the procedure that was used for the initial measurements of the shock switch.

Hardware Turn-on Sequence

1. PXI chassis
2. Computer
3. Power supply (bottom rack), nanocube controller, etc.
4. Software

Measurement Procedure

1. Install sensor, preferably with a fib-milled cylindrical diamond tip, in the IFM head.
2. Mount the die to the aluminum sample holder. Currently, sticky tabs have been used to secure the die to the sample holder. Super glue is not recommended because it could strain the die and degrade the performance of the switch.
3. Attach the sample holder to the nanocube.
4. Turn on the system using sequence described above.
5. In the software, go to Sensor Setup / Transient Response. Laser intensity on each pad should be 2-3V. Below 2V could indicate a problem.
6. In the software go to Sensor Setup/Interference Pattern.
7. Laser 1 and Laser 2 indicators should be on, if not press the indicator. If they still are not on there could be a problem with the lasers. Check the laser power monitor indicator in the Settings Tab (clicking button gives specs if lasers are receiving power; can check against specs or adjust trim pots on laser controller board as needed).
8. Setup the interference pattern measurement.
    a. Initial parameters to try
        i. 250 data points
        ii. 0 Volts for V0 pad 1 and V0 pad 2
        iii. 10V for Vmax Pad 1 and Vmax Pad 2
        iv. 10 for Amp Pad 1 and Amp Pad 2 (this is the gain of the pad voltage amplifier)

v. 1 cylce

b. Press Start

c. Evaluate the interference pattern and then increase Vmax 1 and 2 and scan again if necessary

d. Both patterns should show about the same number of fringes and have somewhere around 2 V P-P

e. Be careful not to increase the Vmax values too high because the sensor can go unstable and snap closed.

f. Balance the sensor by adjusting the V0's until a good interference pattern can be seen on each pad. One wants constant amplitude. You may need to pick intermediate values for V0, since they do not operate independently.

g. If the sensor snaps closed, you can tap on the top plate with a tweezers to get it to break loose.

9. Tune the PID loops for the sensor (open Transient Response tab)

a. Start with Pad 1

b. Set the Setpoint Value and the Manual Output value to the desired point on the interference pattern.

c. Output scalar should be set to 1

d. Reset disables the I and D gains to 0

e. Manual disables the PID and holds a constant voltage on the pad

f. Diode sign should be set to on

g. Output High (V) and Output Low (V) should be set to limit the voltage range PID output

h. Static Gain should be set to 10 for the current electronics

i. Dynamic Gain can be set to either 1 or 10

j. Cycle time sets the frequency of the square wave modulation of the setpoint for tuning

k. Setpoint Step sets the amplitude of the square wave modulation

l. Sample Int sets the data point sampling interval

m. Tune starts the tuning process by modulating the setpoint. Only 1 tab (pad) can be tuned at a time.

n. Naverage does not work correctly. Keep set at zero

o. Loop time sets the pid control loop update interval. Actual loop time is an indicator of the actual loop update interval.

p. I gain is in microseconds

q. Tune the PID gains for the desired transient response.

r. After setting the gain values, zero the Pad Output (V) (output of the PID) by adjusting the Manual Output (V)

s. Repeat for Pad 2.

10. Set up the piezo tube for seek

a. P = 10, I = 3000, D = 0

b. Setpoint =0.2

c. Manual Output =0

d. Output Scalar =1

e. Reset = OFF

f. Manual = ON

g. Phase=OFF

h. Diode Sign=OFF

i. Output High (V) = 10

j. Output Low (V)=-10

k. Static Gain=1

l. Dynamic Gain=1

m. Cycle Time=200

n. Setpoint Step=0

o. Sample Int (ms)=0.2

p. Naverage piezo=0

q. Loop time =10

r. Tune=OFF

s. Hold=OFF

11. Wait at least 20 minutes between steps 9 and 12, or after changing the bias voltage(s), to allow the sensor to stabilize before beginning a force measurement.

12. Position the desired shock sensor tab behind the tip using the XYZ stage controller. Be careful not to crash the tip into the surface.

13. Setup Seek in IFM Measurement tab

    a. Mode=Force

    b. Setpoint (V)=0.2

    c. Piezo Range (nm) =1500

    d. Forward Step Size=1

    e. Backward Step Size=10

    f. Stage Displacement (nm)=500 (should be less than piezo range ~ 1.5 um)

    g. Press Seek

    h. When Piezo detects the surface it will enable the feedback on the piezo and hover.

    i. Check that the feedback is engaged by starting the tune process for the piezo.

    j. Set Manual Output (V) to zero.

    k. Turn Manual switch to ON

14. Go to IFM Measurement/Shock Sensor Cycle Test (note: abort button may not operate; there is currently no check for exceeding a maximum force.)

    a. First, manually seek the push tab of the first stable position (FSP)

        i. Set the number of cycles to zero.

        ii. Enter the current stage coordinates into FSP Device Coordinates

        iii. Set the translation retract distance to 25 µm

        iv. Set the Measurement retract distance to 3µm

        v. Set Maximum Displacement FSP to -5µm

        vi. Set Displacement rate to 0.5µm/sec

        vii. Set #of data points to 1000

viii. Set # to average to 1000

ix. Press Start

x. If no force is detected, move the y stage 5µm and go back to step i

xi. If a force is detected, (indicating contact with the push tab has occurred), increase the Maximum Displacement and try again to push the switch through the point of instability

xii. Record the coordinates of the FSP and the maximum displacement

xiii. Move the stage so that the SSP is near the tip.

xiv. Repeat the above procedure entering the new coordinates in the box for FSP and changing Maximum Displacement (µm) FSP to 5µm

xv. Record the coordinates and maximum displacement for the SSP

xvi. Setup the cycle test by entering the recorded coordinates and displacements in the appropriate boxes and set the number of cycles.

xvii. Cycle starts at the FSP and data is stored automatically.

15. Mutitest mode was being setup to automate the process of making the measurements on the shock sensor but it is just in the early stages. Currently it just loads a text file containing all of the test parameters for a series of measurements.

16. Nanocube Raster scan is used for contact mode topographical imaging of the sample. This functionality seems to be working pretty well.

17. Piezo Raster Scan is used for contact mode topographical imaging of the sample. This functionality works but still needs some testing for verification.

18. Turn off the hardware using the sequence below.

Currently the software outputs the displacement and the voltages applied to the two capacitor pads. These must be scaled to compensate for the voltage divider on the output of the op-amp that drives the pads. The voltage divider is approximately 17.9:1.

Hardware Turn-off Sequence

1. Software. Caution: Turn off lasers with software if going to turn off main power supply to avoid damaging lasers.

2. Computer

3. PXI chassis (optional)

APPENDIX B: VIS IMPLEMENTED IN CONTROL SOFTWARE

The following is a brief description of the primary, LabView VIs used to control the software for the measurements herein. Only VIs that were tested and used for these measurements are listed. The application build used for these measurements is located in Z:\IFM Software\builds\IFM2\ProbeView 3 Installer.

main.vi

This is the primary vi. This vi process all user input to the program and manages the display of information in the user interface. Upon execution, this vi initializes the hardware and launches several background vi's to process the measurement tasks. The main.vi interacts with the background vi's through notifications and data is transferred via a global variable vi.

The event structure in the primary while loop in this vi processes the user events and executes a corresponding piece of code. The timeout case of this structure handles the interaction with background events including status updates and real-time display of measurement data.

fiber light intensity.vi

This vi sets the intensity of Fiber-Lite DC-950 by setting the value of DAC AO6 on the PXI-6704 module.

fiber light power.vi

This vi turns on/off the Fiber-Lite DC-950 by setting the value of Port0/Line1 on the PXI-6704 module.

flatten.vi

This vi is used for the display of raster scan image data. It performs a linear fit to the scan line and subtracts that to correct for tilt.

gen scan arrays.vi

This vi generates the scan arrays for piezo raster scans based on the number of pixels in the image and the scan size.

get frame.vi

This vi handles the interaction with the IEEE-1394 cameras and displays the images on the screen. This vi is setup to work with 2 cameras (e.g., tip view and top view).

The timeout case grabs the image data from the camera and overlays the crosshair on the image. It also manages the recording of video files in avi format.

global variables.vi

The global variables vi is used as an intermediary to transfer data between the main vi and the sub vi's running in the background.

mosaic new.vi

This vi uses the course positioning stages to scan the sample under the optical microscope and generate a tiled image of a larger area of the sample than the field of view of the optics.

move xy to start image.vi

This vi is used to gradually move to the corner of the scan area prior to starting the raster scan. This is done to minimize damage to the tip or sample as well as to reduce the chance "fringe hopping".

real to pixels.vi

Determines the image pixel coordinates from the xy coordinates of the stages.

rectangle overlay.vi

Overlays a rectangle on an image.

setup daq scan.vi

Setup the analog output scanning operation for piezo raster scan.

trigger.vi

This vi is used to initiate analog input and output scanning operations. It sends a digital pulse on port1/line1 of the PXI-6289 module.

xyz stage controller.vi

This vi is used for positioning and display of the xyz course positioning system. The names of the stages are read from the file stages.dat.

auto interference.vi

This vi scans the pad voltages and records the intensity from the photodetectors and records the data to a file. During the scan, the data is written to a global variable for real-time display.

nc move xy to start image.vi

This vi is used to gradually move to the corner of the scan area prior to starting the raster scan. This is done to minimize damage to the tip or sample as well as to reduce the chance "fringe hopping".

nc gen scan arrays.vi

This vi generates the scan arrays for nanocube raster scans based on the number of pixels in the image and the scan size.

nc setup daq scan.vi

Setup the analog output scanning operation for nanocube raster scan.

seek.vi

This vi performs the surface seeking routine and reports status information back to main.vi.

Laser 1 Enable Button.vi

Sends the signal to enable/disable laser number 1.

Laser 0 Enable Button.vi

Sends the signal to enable/disable laser number 0.

File Name.vi

Generates a file name based on the current system time.

mforceprofile.vi

This vi performs the measurements of force profiles. It runs in the background and waits for notifications from main.vi to start a measurement. It reports status information back to main.vi through notifiers and global variables for real-time display. The notification, "Lateral Force Nanocube", is used for shock switch measurements. Normal Force piezo has been used some for normal force profiles but probably needs more testing and verification.

laser monitors.vi

Reads and displays values for current, power, current limit, and power limit.

Generate ramp.vi

Generates piezo voltage ramp for nforce piezo.vi.

Setup output scan.vi

Sets up the output scan for nforce piezo.vi

Setup input scan.vi

Sets up the input scan for nforce piezo.vi

Start trigger.vi

Triggers the input and output scan operations to begin in nforce piezo.vi.

nforce piezo.vi

Sub vi called from the mforceprofile vi to make a normal force profile measurement.

Linfit waveform.vi

Sub vi called from nforce piezo.vi to do a linear fit to a waveform. Before starting a force profile, the force is recorded over a set time interval and fits to a line to estimate the drift rate in the force measurement. This drift rate is stored with the profile data.

Retract tip.vi

Retracts tip and disables the hover.

Convert n force.vi

Calculates the normal force based on the pad voltages.

read stage and optics file.vi

Reads the text file stages.dat to configure the system for the stages that are connected.

nforce profile header.vi

Writes the header for the normal force profile data files.

ncube image header.vi

Writes the header information for the nanocube image files.

shutdown.vi

Prepares the system for shutdown when exiting the application.

E-710 nanocube controller RS232 com.vi

This vi is a test vi for checking communication with the E-710 nanocube controller. It allows basic movement capabilities and monitors the position of the nanocube.

plot interference.vi

This vi allows the user to overlay several interference patterns on a single graph.

Shock Switch analysis

This vi is used for analyzing the shock switch data and merging the two parts of the measurement cycle.

FPGA PID.vi

This is the main program running on the FPGA for the PID loops for the sensor and the piezo. Averaging should not be used. PID 1, 2 are for the sensor feedback loops. Pid3 is not used. PID 4 is for the piezo tube and PID5 is for the nanocube. PID 5 did not work very well because it is bit limited. PID SubVI performs the PID calculations for the sensor. PID SubVI piezo performs the calculations for the piezo tube. The input and outputs of the PID loops are transfer to the host vi through DMA channels. If modifying this VI, it must be compiled and uploaded to the FPGA, and linked to the software.

Distribution

1 National Institute of Standards
Attn: Jon R. Pratt
100 Bureau Drive, Stop 8221
Gaithersburg, MD 20899-8221

1	MS0665	Eric Detlefs	2541
1	MS0899	Technical Library	9536 (electronic copy)
1	MS0899	Technical Library	4536
1	MS1056	David Sandison	1110
1	MS1069	Michael S. Baker	1749
1	MS1080	Keith Ortiz	1749
1	MS1322	John A. Mitchell	2614
1	MS1415	Carlos Gutierrez	1114
1	MS1415	Nathan Moore	1114
1	MS1415	Jack E. Houston	1114
2	MS9018	Central Technical Files	8944


Sandia National Laboratories